Toward two-phase simulation of the primary breakup of a round liquid jet by a coaxial flow of gas

By D. Kim, O. Desjardins, M. Herrmann AND P. Moin

1. Motivation and objectives

Two-phase flows are very common in nature and technical processes such as ocean waves, tire splash, and combustion devices. Among them, the atomization of liquid jets or sheets by gas streams has received much attention due to its direct applicability to the design of combustion chambers. However, it is challenging to model such a phenomenon because of its complex nature. In a combustion chamber, fuel is typically injected as a liquid and atomized subsequently to enhance evaporation. Combustion then occurs in the gaseous phase. Atomization involves a sudden jump in the density across the interface, surface tension force on the interface, topological changes of the interface, and phase transition. Moreover, atomization of the liquid jet usually occurs in a turbulent environment.

The atomization of a liquid jet can be considered as two subsequent processes, i.e., primary atomization followed by secondary atomization. The primary atomization is the initial breakup of the liquid jet into large and small liquid structures close to the injection nozzle. It involves complex interface topology of large coherent liquid structures. The secondary atomization is the subsequent breakup into smaller drops forming sprays. For the secondary atomization, a number of breakup models for liquid drops have been proposed and validated (Reitz 1987; Tanner 1997; Apte *et al.* 2003). Using these breakup models, there have been several attempts to simulate a liquid jet injected into a chamber by representing the liquid core by a collection of liquid drops. However, the results are easily changed by the initial drop size distribution, which is unknown without appropriate primary atomization modelling. Although primary atomization is necessary to simulate the whole atomization process, modelling still remains a major unresolved problem. It is, therefore, crucial to develop a feasible high-fidelity computational tool for simulation of the whole primary and secondary atomization process.

In this study, we conduct numerical simulations to investigate the breakup mechanism of a liquid jet surrounded by a coaxial flow of gas. A Refined Level Set Grid (RLSG) method (Herrmann 2004; 2005; 2006) coupled to a Lagrangian spray model (Apte *et al.* 2003) is used to capture the whole breakup process of the liquid jet. In the near field of the liquid jet, where the primary breakup occurs, motion and topological changes of the liquid jet are described by the RLSG method. In this region, a liquid jet consists of the core and ligaments, which subsequently break into drops of various sizes. The drops generated by the primary breakup are transferred to a Lagrangian spray model in order to describe the secondary breakup process.

2. Numerical methods

2.1. *Governing equations*

The Navier-Stokes equations for incompressible, immiscible, two-phase flow are described as

$$\rho\frac{\partial \mathbf{u}}{\partial t} + \rho\mathbf{u}\cdot\nabla\mathbf{u} = -\nabla\mathbf{p} + \nabla\cdot\tau + \mathbf{T}_\sigma \tag{2.1}$$

$$\nabla\cdot\mathbf{u} = \mathbf{0}, \tag{2.2}$$

where ρ is the density, p is the pressure, τ is the viscous stress tensor, and $\mathbf{T}_\sigma$ is the surface tension force.

A level set method is applied to track the location of the phase interface. The location and time evolution of the phase interface are described by the level set equation:

$$\frac{\partial G}{\partial t} + \mathbf{u}\cdot\nabla G = 0, \tag{2.3}$$

where the isosurface $G = 0$ defines the location of the interface, $G > 0$ in the liquid, and $G < 0$ in the gas phase. In the computational domain, G is set to be a signed distance function to the interface:

$$|\nabla G| = 1. \tag{2.4}$$

The interface normal vector $\mathbf{n}$ and the interface curvature κ can be calculated as

$$\mathbf{n} = \frac{\nabla G}{|\nabla G|}, \tag{2.5}$$

$$\kappa = \nabla\cdot\mathbf{n}. \tag{2.6}$$

In this paper, we used the RLSG method to solve the coupled level set equations (2.3, 2.4). The level set transport equation (2.3) is solved on a separate refined G-grid using fifth-order WENO scheme (Jiang & Peng 2000) with a third-order TVD Runge-Kutta time discretization (Shu & Osher 1989). It is coupled to the flow solver through $\mathbf{u}$. The velocity $\mathbf{u}$ on the fine G-grid is obtained by trilinear interpolation from the flow solver grid. Reinitialization (2.4) is solved by an iterative procedure using a fifth-order WENO scheme and a first-order pseudo-time integration (Sussmann *et al.* 1994; Peng *et al.* 1999). The numerical details about the RLSG method are described in Herrmann (2005; 2006).

In order to solve the flow-field, an unstructured grid solver is used based on a balanced force finite volume formulation of the variable density Navier-Stokes equations (Mahesh *et al.* 2004; Ham & Iaccarino 2004; Herrmann 2006). The Navier-Stokes equations (2.1) are coupled to the level set equation (2.3) through the density, viscosity, and surface tension force. The density ρ and the viscosity μ in a cell i are defined as volume averaged quantities:

$$\rho_i = \psi_i\rho_l + (1-\psi_i)\rho_g \tag{2.7}$$

$$\mu_i = \psi_i\mu_l + (1-\psi_i)\mu_g, \tag{2.8}$$

where the subscript l denotes quantities in the liquid and the subscript g denotes those in the gas phase. The flow solver volume fraction ψ is defined as

$$\psi_i = \frac{1}{V_i}\int_{V_i} H(G)dV, \tag{2.9}$$

where H is the Heaviside function and V_i is the control volume of the flow solver grid cell. In the RLSG method, this integral is calculated on the G-grid as

$$\frac{1}{V_i}\int_{V_i} H(G)dV = \frac{\sum_{i_G}\psi_{i_G}V_{i,i_G}}{\sum_{i_G}V_{i,i_G}} \tag{2.10}$$

where V_{i,i_G} is the joined intersection volume of the G-grid cell i_G and the flow solver control volume V_i, and the G-grid volume fraction ψ_{i_G} is calculated using an analytical formula developed by van der Pijl *et al.* (2005),

$$\psi_{i_G} = f(G_{i_G}, \mathbf{n}_{i_G}). \tag{2.11}$$

The surface tension force $\mathbf{T}_\sigma$ is calculated as

$$\mathbf{T}_{\sigma,i} = \int_{V_i} \sigma\kappa\nabla\psi d\mathbf{x}, \tag{2.12}$$

where σ is the surface tension force coefficient. The curvature κ is transferred from the G-grid to the flow solver grid,

$$\kappa = \frac{\sum_{i_G}V_{i,i_G}\delta_{i_G}\kappa_{i_G}}{\sum_{i_G}V_{i,i_G}\delta_{i_G}}, \tag{2.13}$$

where $\delta_{i_G} = 0$ if $\psi_{i_G} = 0$ or $\psi_{i_G} = 1$, and $\delta_{i_G} = 1$ otherwise. Details of the balanced force algorithm and curvature are described in Herrmann (2006).

2.2. *Coupling to flow solver*

In this work, the RLSG method has been coded in a separate solver called LIT (Level set Interface Tracker). All communication between the level set solver and the flow solver is handled by a coupling software, named CHIMPS (Coupler for High-performance Integrated Multi-Physics Simulations, Alonso *et al.* 2006). CHIMPS is used for all interpolation of velocity vectors from the flow solver grid to the G-grid and all volume integration from the G-grid to the flow solver grid. The advantage of this approach is that any flow solver can be coupled to LIT. In this study, LIT has been coupled to CDP, a fully unstructured, LES flow solver (Ham & Iaccarino 2004; Mahesh *et al.* 2005; Herrmann 2006).

2.3. *Drop transfer*

A vast number of atomized drops can be generated in the atomization process of liquid jets. Thus, it becomes prohibitively expensive to resolve every drop by the level set scalar. Instead, Lagrangian spray models are more adequate to describe small scale liquid drops having simple geometry. In this study, broken small liquid drops are identified, removed from the level set representation, and inserted as liquid drops into a Lagrangian spray model if they satisfy the two criteria presented below.

In order to identify the broken-off drops, special care must be taken because broken liquid structures can span different blocks on different processors. The drop identification algorithm with multi-block domain decomposition is fully explained in Herrmann (2005).

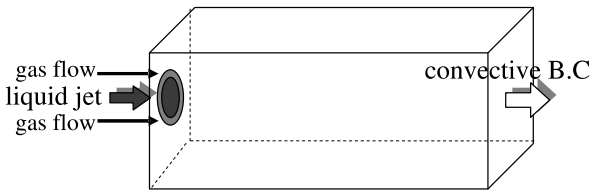

FIGURE 1. Computational domain of a round liquid jet surrounded by a coaxial flow of gas.

Using this algorithm, the volume of a broken drop and its center of mass can be easily calculated.

As previously mentioned, there are two criteria for drop transfer. The first one states that the drop volume V_D has to be smaller than the volume criterion for a Lagrangian spray model,

$$V_D \leq V_{D_{max}}, \tag{2.14}$$

with $V_{D_{max}}$ proportional to the volume of the local flow solver grid cell volume V_i. Since the RLSG method can provide subgrid resolution with respect to the flow solver grid, broken-off liquid structures whose volumes are less than V_i are still resolved, can be identified and are candidates for Lagrangian spray tracking. The second criterion is a shape criterion. Although a broken-off liquid structure might satisfy the above volume criterion, it should not be transferred to the Lagrangian spray model if its shape is not spherical, for example, if it is a thin ligament. The spherical shape criterion is defined as

$$r_{max} < 2r_{sphere}, \tag{2.15}$$

where r_{max} is the maximum distance between the center of mass and the surface of the drop and r_{sphere} is the radius of a sphere such that $4/3\pi r^3_{sphere} = V_D$. If both criteria are satisfied, the liquid drop is removed from the level set tracked representation and inserted into the Lagrangian spray model, preserving its mass, center of mass, and momentum.

3. Results

When a liquid jet flows in a faster coaxial gas stream, different atomization regimes are observed depending on Weber numbers and the velocity difference between the liquid and gas (Farago & Chigier 1992; Zaleski *et al.* 1996). At low gas velocity, a liquid jet wanders in the gas stream, inducing bags and rims. For higher gas velocities, the liquid jet is no longer deformed as a whole, but it is peeled off at its surface forming ligaments. These ligaments are broken into small liquid droplets. The typical droplet size decreases with the velocity difference (Yatsuyanagi *et al.* 1994,; Lasheras *et al* 1998). The drop size distribution shows an exponential tail characteristic of broad size statistics and is very important for industrial applications.

Recently, Marmottant and Villermaux (2004) performed various experiments on the atomization of a liquid jet when a gas stream flows coaxial to its surface. Their experimental findings suggest that two successive instabilities are responsible for the disintegration of the liquid jet into dispersed droplets. First, a Kelvin-Helmholtz type instability triggers axisymmetric modulations on the liquid by shear between the slow liquid and the fast gas stream. Then, these axisymmetric waves undergo transverse azimuthal modulations when the gas velocity goes beyond a critical velocity. This azimuthal secondary instabil-

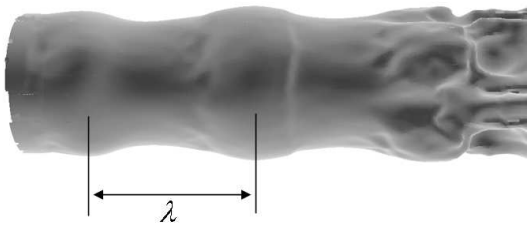

FIGURE 2. Axisymmetric modulation on the liquid surface at the initial stage of the breakup.

ity of the axisymmetric waves was explained by the Rayleigh-Taylor instability in their study (Marmottant & Villermaux 2004). At azimuthal wave crests, liquid ligaments are produced, elongated by the gas stream, and finally broken into droplets.

In this section, we investigate these two instabilities responsible for the droplet formation from a round liquid jet and examine the statistical property of the resulting droplets for different G-grid resolutions.

3.1. *Computational details*

A round liquid jet surrounded by a coaxial flow of gas is simulated as shown in Fig. 1. The liquid jet is injected at the center with the nozzle diameter D. The surrounding gas flows coaxially with the annular gap thickness h. The gap thickness h is $0.3D$. In this paper, the jet parameters are determined following the experiment of Marmorttant & Villermaux (2004). However, the density ratio of the liquid and gas is limited to 5. The Reynolds and Weber numbers of the gas based on the gap thickness h are $Re_g = u_g h/\nu_g = 3770$ and $We_g = \rho_g h u_g^2/\sigma = 34$, respectively, which are the same values in the experiment. The Reynolds and Weber numbers of the liquid are $Re_l = u_l D/\nu_l = 295$ and $We_l = \rho_l D u_l^2/\sigma = 0.6$, respectively, based on the liquid jet velocity and D. The momentum ratio used is $\rho_l u_l^2/\rho_g u_g^2 = 190$. An error function is used for the velocity profile of the gas and the liquid at inlets. The inlet boundary-layer thickness of the gas δ_g is $0.096D$; that of the liquid δ_l is determined by

$$\delta_l = \sqrt{\frac{\mu_l \rho_g}{\mu_g \rho_l}}\delta_g. \tag{3.1}$$

The boundary-layer thickness used in this study is larger than that in the experiment of Marmorttant & Villermaux (2004) due to the available grid resolution.

The size of the computational domain used is $-2.5 < x/D < 2.5$, $-2.5 < y/D < 2.5$, and $0 < z/D < 8$. Slip boundary conditions are used except at the jet inlet and exit boundary, and convective boundary conditions are used for the exit boundary. Uniform Cartesian meshes are used for the flow solver and level set solver grids. The grid size for the flow solver is $\Delta x/D = 0.02$. For the level set solver, we used two different G-grids: $\Delta_G/D = 0.02$ and $\Delta_G/D = 0.01$. The velocity profiles of the gas and the liquid at the inlet are used for the initial velocity field along the jet direction.

3.2. *Kelvin-Helmholtz instability*

Figure 2 shows the axisymmetric modulation on the liquid jet at the initial stage. Two fluids having different velocities are inherently unstable, producing an instability of the Kelvin-Helmholtz type. From the stability analysis by Villermaux (1998), the selected

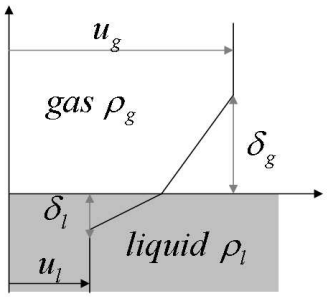

FIGURE 3. Linear velocity profile used in the Kelvin-Helmholtz stability analysis.

wavelength and frequency at the maximum growth rate are expressed as a function of the density ratio and gas boundary-layer thickness δ_g when a linear velocity profile is assumed (Fig. 3):

$$\lambda_{kh} = \frac{2\pi}{0.8} F(\frac{\rho_l}{\rho_g})\delta_g, \tag{3.2}$$

where $F(\rho_l/\rho_g)$ is

$$F(\frac{\rho_l}{\rho_g}) = \frac{5}{6} - \frac{1}{6(\rho_l/\rho_g)} + \frac{\sqrt{5 + 13(\rho_l/\rho_g) - 37(\rho_l/\rho_g)^2 + 27(\rho_l/\rho_g)^3}}{6\sqrt{2}(\rho_l/\rho_g)}. \tag{3.3}$$

The group velocity of the most amplified wavenumber is well estimated by a convection velocity u_c as

$$u_c = \frac{\sqrt{\rho_1}u_1 + \sqrt{\rho_2}u_2}{\sqrt{\rho_1} + \sqrt{\rho_2}}. \tag{3.4}$$

Thus, the period of the surface modulation T_{kh} is given by

$$T_{kh} = \frac{1}{f_{kh}} = \frac{u_c}{\lambda_{kh}}. \tag{3.5}$$

From the computational result, the wavelength is measured as the mean distance between the highest point of the primary waves and the frequency is measured by calculating the mean velocity of the wave crests. Table 1 shows the wavelength and period divided by those obtained from the stability analysis, respectively. Experimental values from Marmorttant & Villermaux (2004) are much smaller than those from the stability analysis since the velocity profile is not linear in the experiments and the effective linear boundary-layer thickness used in the stability analysis is much larger than the experiment as mentioned in Marmorttant & Villermaux (2004). However, the boundary-layer thickness used in this study is 4 times larger than the experiment. Therefore, our results are much closer to the stability analysis than the experiment.

3.3. *Raleigh-Taylor instability*

After the onset of shear instability causing axisymmetric waves, transverse azimuthal modulations appear as shown in Fig. 4. Several mechanisms have been suggested to explain these modulations. Villermaux and Clanet (2002) have proposed that transient

Table 1. Comparison of the wavelength and period of the primary modulation.

	Experiments (Marmottant *et al.* 2004)	Present study	Stability analysis
Wavelength λ/λ_{kh}	0.29	0.83	1.0
Period T/T_{kh}	0.33	0.85	1.0

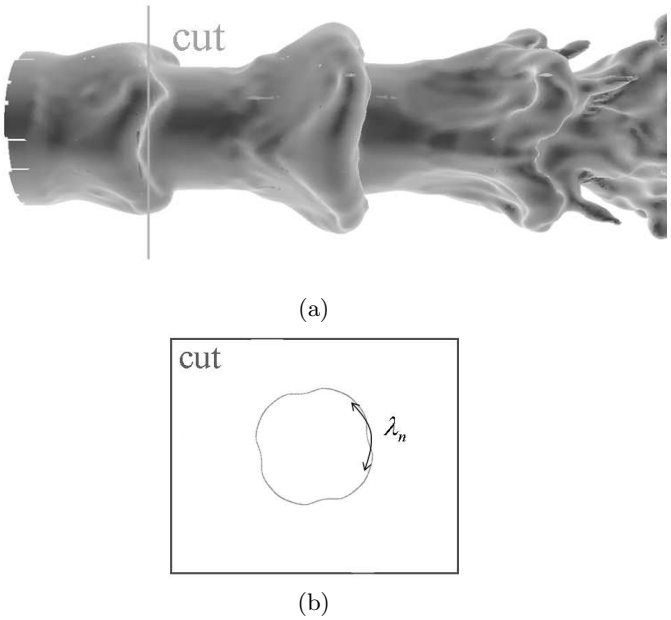

FIGURE 4. (a) Transverse azimuthal modulations on the liquid surface; (b) liquid interface in the cutting plane.

acceleration in the direction normal to the liquid at the rims triggers a Rayleigh-Taylor instability, which produces the azimuthal perturbation.

The most amplified wavenumber k_m can be calculated by (Chandrasekhar 1961)

$$k_m = \left[\frac{(\rho_2 - \rho_1)g}{3\sigma}\right]^{1/2}, \tag{3.6}$$

where g is the maximum acceleration of the primary wave expressed as

$$g = a\left(2\pi\frac{u_c - u_1}{\lambda_{kh}}\right)^2, \tag{3.7}$$

with a the amplitude of the primary wave. By this stability analysis, the theoretical wavelength for our simulated condition is approximately $0.72D$, which means four crests are triggered on the primary wave rims. As shown in Fig. 4(b), our computational result is consistent with the stability analysis showing exactly four crests.

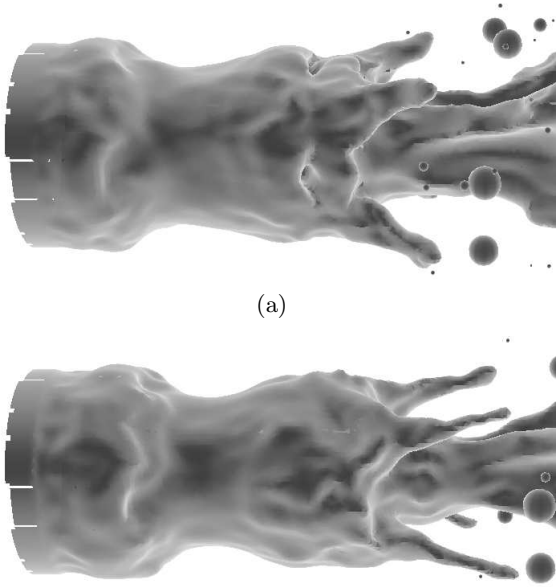

(a)

(b)

FIGURE 5. (a) Development of the ligaments; (b) further elongation of the ligaments.

3.4. *Ligament development and breakup*

The transverse azimuthal modulations grow in amplitude producing small ligaments at the wave crests. These are elongated further by the gas stream and their diameter decreases as shown in Fig. 5. The ligaments are finally pinched off, usually at their base, and broken into liquid droplets. When the ligaments are detached, a capillary instability grows in a very short time and breaks them into several droplets of different sizes (Fig. 6). These droplets are automatically transferred to the Lagrangian spray model through our drop transfer algorithm (Fig. 6(b)).

3.5. *Drop formation*

Several drops are formed from the detached ligaments. In natural spray formation, drops, such as rain drops and fuel droplets, have a broad range of sizes. The statistical drop size distribution has been known to show an exponential tail shape.

In the computational simulations, level set tracked liquid droplets smaller than the G-grid resolution cannot be resolved correctly. Thus, drop size distributions at small scales of the order of the G-grid resolution can be expected to be dependent on the grid resolution and should be considered a numerical artifact. It is, therefore, important to determine a converged drop diameter d_c, i.e., the drop size above which the drop size distribution is statistically converged and grid-independent.

Figure 7 shows the drop size distribution with two different G-grid resolutions. The flow solver grid resolution is fixed to $\Delta x/D = 0.02$. As shown in Fig. 7, the peaks in the number of drops show a large difference between the two grids. However, the drop size distributions at larger diameters have a similar shape. Thus, we can consider the converged drop diameter to be approximately $d_c = 0.04D$. In terms of the G-grid resolution $\Delta_G = 0.02$, the converged drop diameter d_c thus corresponds to $d_c = 2\Delta_G$. Any drops produced with a diameter smaller than d_c ought to be considered a numerical

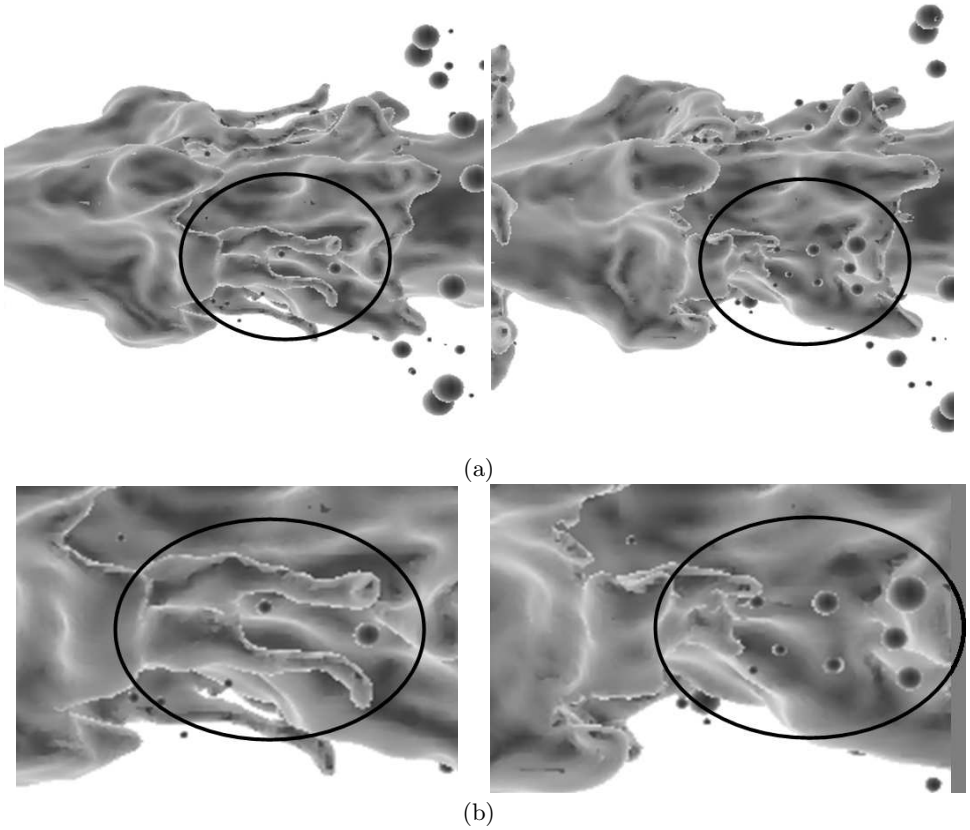

FIGURE 6. (a) Formation of the droplet from the ligaments; (b) zoom on the ligament-breakup region: liquid jet structures such as ligaments are tracked by the level set method and shaded spherical objects are Lagrangian sprays.

artifact and cannot be trusted. Therefore, the concept of a converged drop diameter provides an important and useful reference for computational simulations.

4. Conclusions and future work

The atomization of a liquid jet surrounded by a coaxial flow of gas was numerically simulated using a Refined Level Set Grid (RLSG) method with a Lagrangian spray model. The characteristics of the underlying breakup mechanism have been examined to show the validity of the simulation. Our results are consistent with the experimentally observed physical mechanisms and the corresponding stability analysis. The drop-size distribution of the resulting spray after breakup exhibits grid-independent results for drops resolved by at least two G-grid cells per diameter. This proves the applicability of our method for simulations of the atomization process of liquid jets.

In this work, the density ratio between the gas and liquid was limited to 5. Future work will focus on the atomization of coaxially atomized liquid jets with higher density ratio and thin boundary-layer thickness using the same parameters as the experiments of Marmottant & Villermaux (2004).

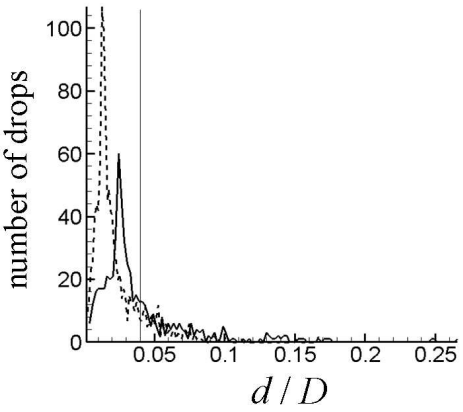

FIGURE 7. Drop size distribution with two different G-grid sizes: ——, $\Delta_G = 0.02$; – – –, $\Delta_G = 0.01$.

Acknowledgments

The work presented in this paper was supported by the Department of Energy's ASC program. The authors also would like to thank F. Ham and S. Apte.

REFERENCES

ALONSO, J. J., HAHN, S., HAM, F., HERRMANN, M., IACCARINO, G., KALITZIN, G., LEGRESLEY, P., MATTSSON, K., MEDIC, G., MOIN, P., PITSCH, H., SCHLÜTER, J., SVÄRD, M., VAN DER WEIDE, E., YOU, D. & WU, X. 2006 CHIMPS: A high-performance scalable module for multi-physics simulations. *AIAA Paper* 2006-5274.

APTE, S. V., GOROKHOVSKI, M. & MOIN, P. 2003 LES of atomizing spray with stochastic modeling of secondary breakup *Int. J. Mult. Flow* **29**, 1503–1522.

CHANDRASEKHAR, S. 1961 Hydrodynamic and hydromanetic stability. *Dover.*

FARAGÓ, Z. & CHIGIER, N. 1992 Morphological classification of disintegration of round liquid jets in a coaxial air stream. *Atom. Sprays* **2**, 137–153.

HAM, F. & IACCARINO, G. 2004 Energy conservation in collocated discretization schemes on unstructured meshes. *Annu. Res. Briefs 2004*, Center for Turbulence Research, 3–14.

HERRMANN, M. 2004 On mass conservation and desingularization of the Level Set/Vortex Sheet method. *Annual Research Briefs 2004*, Center for Turbulence Research, 15–30.

HERRMANN, M. 2005 Refined Level Set Grid method for tracking interfaces. *Annual Research Briefs 2005*, Center for Turbulence Research, 3–18.

HERRMANN, M. 2006 A balanced force refined levle set grid method for two-phase flows on unstructured flow solver grids. *Annual Research Briefs 2006*, Center for Turbulence Research.

JIANG, G.-S. & PENG, D. 2000 Weighted ENO schems for Hamilton-Jacobi equations. *SIAM J. Sci. Comp.* **21**, 2126–2143.

Lasheras, J., Villermaux, E. & Hopfinger, E. 1998 Breakup and atomization of a round water jet by a high-speed annular jet. *J. Fluid Mech.* **357**, 351–379.

Mahesh, K., Constantinescu, G. & Moin, P. 2004 A numerical method for large eddy simulation in complex geometries. *J. Comput. Phys.* **197**, 215–240.

Marmottant, P. & Villermaux, E. 2004 On spray formation *J. Fluid Mech.* **498** 73–111.

Peng, D., Merriman, B., Osher, S., Zhao, H. & Kang, M. 1999 A PDE-based fast local level set method. *J. Comput. Phys.* **155**, 410–438.

Shu, C.-W. & Osher, S. 1989 Efficient implementation of essentially non-oscillatory shock-capturing schemes. *J. Comput. Phys.* **77**, 439–471.

Villermaux, E, 1998 On the role of viscosity in shear instabilities. *Phys. Fluids* **10**, 368–373.

Van Der Pikl, S. P., Segal, A. & Vuik, C. 2005 A mass-conserving level-set method for modelling of multi-phase flows. *Int. J. Numer. Meth. Fluids* **47**, 339–361.

Yatsuyanagi, N., Sakamoto, H. & Sato, K. 1994 Atomization characteristics of liquid jets injected into a high-velocity flow field. *Atom. Sprays* **4**, 451–471.

Zaleski, S., Li, J., Scardovelli, R. & Zanetti, G. 1996 Direct simulation of multiphase flows with density variations. *In Colloque IUTAM on Variable Density Low Speed Turbulent Flows, Marseille 8–10 Juillet 1996* (ed. L. Fulachier & F. Anselmet). Kluwer.